RPE | Radiation Physics & Engineering
A Peer-Reviewed Journal
Published by K.N. Toosi University of Technology
http://rpe.kntu.ac.ir
Research Article

Radiation Physics and Engineering 2025; 6(3):9–16

Nuclear symmetry energy and its role in the thermodynamic instabilities of nuclear matter using an ab initio statistical approach

Seyyed Alireza Ghaemmaghami, Mehdi Ghazanfari Mojarrad*
Department of Physics, Faculty of Science, University of Kashan, Kashan, Iran

HIGHLIGHTS

- The effect of symmetry energy on thermodynamic instabilities of nuclear matter.
- Comparison of Seyler-Blanchard and Myers-Swiatecki interactions in thermodynamic properties of nuclear matter.
- Temperature plays a dominant role in eliminating the instability region.
- The instabilities of asymmetric nuclear matter coincide in both the chemical and mechanical modes.
- The mechanical instabilities play a dominant role in thermodynamic instabilities.

ABSTRACT

In this research, by using the Seyler-Blanchard (SB) interaction, we present the Thomas-Fermi statistical approach in the simplest possible form in order to study the thermodynamic properties of nuclear matter with special attention to symmetry energy and its role in the thermodynamic instabilities. Our results show that the symmetry energy and symmetry free energy for the SB interaction are stiffer than those for the Myers-Swiatecki (MS) interactions. It can be seen that the temperature plays a prominent role in eliminating the unstable regions of the phase diagrams so that the unstable region shrinks with increasing temperature until it disappears at the critical temperature. Furthermore, the thermodynamic instabilities of asymmetric nuclear matter (ANM) occur simultaneously in both the chemical and mechanical modes, while the mechanical instabilities play a dominant role, as can be observed more significantly in the SB interaction than in the MS interactions due to the stiffer behavior of the symmetry energy and the symmetry free energy. This work paves the way for in-depth research on the liquid-gas phase transition, considering that the other theoretical predictions are consistent with the results of this model.

KEYWORDS

Thomas-Fermi
Nuclear matter
Seyler-Blanchard interaction
Symmetry energy
Symmetry free energy
Thermodynamic instabilities

HISTORY

Received: 5 May 2024
Revised: 4 November 2024
Accepted: 21 December 2024
Published: Summer 2025

1 Introduction

A supernova explosion (Prakash et al., 1997; Pons et al., 1999; Strobel and Weigel, 2001; Camenzind, 2007; Hempel et al., 2012; Moshfegh and Ghazanfari Mojarrad, 2013) accompanied by core collapse is widely regarded as a unique natural laboratory for the study of thermodynamic properties of nuclear matter at high temperatures and densities. Nuclear matter is a hypothetical and ideal system with numerous nucleons, where interactions are predominantly dictated by the nuclear force, with Coulomb interactions between nucleons being disregarded. Nuclear matter is described by baryon density $\rho = \rho_n - \rho_p$ and asymmetric parameter $\delta = \frac{\rho_n - \rho_p}{\rho}$, which is for symmetric nuclear matter (SNM) $\delta = 0$, asymmetric nuclear matter (ANM) $0 < \delta < 1$, and pure nuclear matter (PNM) $\delta = 1$.

In the exploration of nuclear matter properties, researchers have introduced different models, which fall into the categories of microscopic (Baldo et al., 2001; Fedoseew and Lenske, 2015; Drischler et al., 2016) or phenomenological (Bandyopadhyay and Samaddar, 1988; Baldo et al., 2001; Drischler et al., 2016; Bandyopadhyay et al., 1990; Myers and Swiatecki, 1990; Xu et al., 2007; Moshfegh and Mojarrad, 2011). This category is based on experimental constraints and the specific type of interaction employed. This classification is based on the experimental constraints and the specific type of interaction employed. Consequently, the nuclear theories have been developed by these models in the recent decades. The micro-

*Corresponding author: ghazanfari@kashanu.ac.ir

https://doi.org/10.22034/rpe.2024.455720.1195

scopic models involve studying nuclear matter properties using potentials de-rived from nucleon-nucleon scattering data. In contrast, the phenomenological models utilize po-tentials compatible with the properties of SNM saturation point and the parameters of the semi-empirical mass formula to determine the equation of state (EOS) of nuclear matter. Although both methods are efficient, we are looking for a method that can achieve the thermodynamic properties of the nuclear matter optimally. For this purpose, we use a phenomenological and statistical model based on the Thomas-Fermi approximation as a mean-field approach. The Thomas-Fermi model was used for the first time in atomic physics, and with the advances made in this theory, it obtained the necessary conditions for use in nuclear physics (Moshfegh and Mojarrad, 2011; Moshfegh and Ghazanfari Mojarrad, 2013; Ghazanfari Mojarrad and Arabsaeidi, 2016; Mojarrad et al., 2018; Mojarrad and Razavi, 2019; Ghazanfari Mojarrad and Ranjbar, 2019; Mojarrad and Ranjbar, 2020; Ranjbar and Ghazanfari Mojarrad, 2021; Razavi and Mojarrad, 2023; Ghaemmaghami and Ghazanfari Mojarrad, 2023; Ghaemmaghami et al., 2023; Ghaemmaghami and Mojarrad, 2022). Based on this model, the interacting particles can be considered pseudo-particles that occupy the available states like a gas in the phase space, assuming the Pauli exclusion principle. Therefore, the momentum and position of the particles determine the state of the particles in the phase space. To present this approach in the framework of the Thomas-Fermi approximation, one can use the fundamental interaction of the Seyler-Blanchard (SB) (Seyler and Blanchard, 1961; Brandow, 1967; Randrup and de Lima Medeiros, 1991; Ghaemmaghami et al., 2023), which can be extended to the density-dependent interaction of Myers-Swiatecki (MS) (Moshfegh and Mojarrad, 2011; Myers and Swiatecki, 1990; Moshfegh and Ghazanfari Mojarrad, 2013), whose parameters can be adjusted to the quantities such as binding energy and saturation density of nuclear matter. Therefore, to generalize the scope of calculations, the SB interaction can be basically employed as an ab initio approach for investigating the thermodynamic properties such as single-particle effective energy, neutron chemical potential, symmetry energy, symmetry free energy, and thermodynamic insta-bilities of nuclear matter at different temperatures and densities. The article is structured as fol-lows: firstly, the formulation of the statistical model based on SB interaction is presented for the study of thermodynamic properties, symmetry energy, symmetry free energy, and thermodynamic instabilities of nuclear matter. In the next section, we discuss the results obtained from this model. Finally, the summary and conclusion are given.

2 Formalism

This study introduces the formalism of nuclear matter, employing the SB interaction fitted with the data of finite nuclei and the saturation properties of nuclear matter (Randrup and de Lima Medeiros, 1991; Ghaemmaghami et al., 2023) within the framework of the Thomas-Fermi approximation:

$$V_{SB}(r_{12},p_{12}) = -C\frac{\mathrm{e}^{-r_{12}/a}}{r_{12}/a}\big(1-\frac{p_{12}^2}{p_b^2}\big) \tag{1}$$

where, the relative position and momentum of each pair of nucleons in the phase space are denoted by r_{12} and p_{12}, respectively. In addition, $C = 453.1$ MeV is the particle interaction strength, a is the Yukawa force range, $p_b = \sqrt{2\bar{m}T_b}$ is the characteristic Fermi momentum with the characteristic kinetic energy $T_b = 89.274$ MeV, and $\bar{m} = 938.903\ \mathrm{MeV.c^{-1}}$ is the average nucleonic mass (Randrup and de Lima Medeiros, 1991; Ghaemmaghami et al., 2023). The nucleonic density, energy density and entropy density of the ith nucleon in this statistical model are derived as follows:

$$\rho = \sum_{i=n,p}\frac{2}{h^3}\int \mathrm{d}^3p_1 n_i(p_1) \tag{2}$$

$$e = \sum_{i=n,p}\frac{2}{h^3}\int \mathrm{d}^3p_1\Big(\frac{p_1^2}{2\bar{m}}+\frac{1}{2}V_{SB}(p_1)\Big)n_i(p_1) \tag{3}$$

$$\begin{aligned} s = -\sum_{i=n,p}\frac{2}{h^3}\Big\{\int \mathrm{d}^3p_1 n_i(p_1)\ln(n_i(p_1)) \\ + (1-n_i(p_1))\ln(1-n_i(p_1))\Big\} \end{aligned} \tag{4}$$

where the occupation number of the ith nucleon in the phase space, determined through the condition of minimizing the grand thermodynamic potential (Ghaemmaghami and Ghazanfari Mojarrad, 2023), is given by:

$$\begin{aligned} n_i(p) &= \big(1+\exp\big[(\epsilon_{ph}(p)-\mu_i)/T\big]\big) \\ \epsilon_{ph}(p) &= \frac{p^2}{2B}+U(p_n,p_p) \end{aligned} \tag{5}$$

with

$$B = \frac{\bar{m}}{1+\dfrac{4\pi a^3 C}{T_b}\rho} \tag{6}$$

$$U(\rho_n,\rho_p) = 4\pi a^3 C(-\rho+k_n+k_p) \tag{7}$$

$$k_i = \frac{2}{h^3}\int \big(\frac{p_1}{p_b}\big)^2 n_i(p_1)\mathrm{d}^3p_1 \tag{8}$$

In the above relations, $\epsilon_{ph}(p)$ denotes the single-particle energy, B signifies the effective mass, $U(p_n,p_p)$ represents the single-particle potential, and μ_i indicates the nucleonic chemical potential. Using the fundamental quantity of Helmholtz free energy density $f = e - Ts$, the pressure can be calculated to determine the EOS of nuclear matter:

$$\begin{aligned} P &= \rho^2\Big(\frac{\partial(\frac{f}{\rho})}{\partial\rho}\Big)_T = \sum_{i=n,p}(\rho_i\mu_i) - f \\ \mu_i &= \frac{\partial f}{\partial p_i} \end{aligned} \tag{9}$$

which can be expressed at zero temperature as follows:

$$P + e = \sum_{i=n,p}(\rho_i\mu_i) \tag{10}$$

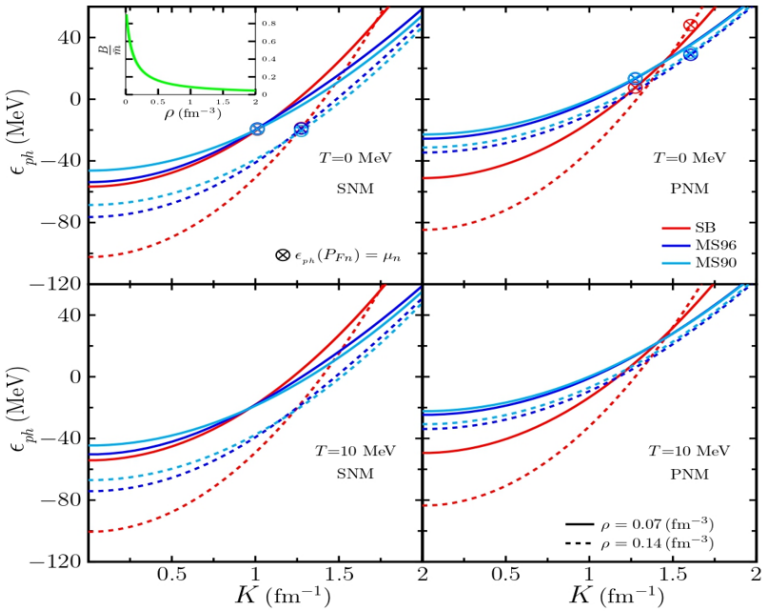

Figure 1: Single particle effective energy ph as a function of wavenumber K at temperature $T = 0$ MeV (top panels) and temperature $T = 10$ MeV (bottom panels) for SNM (left panels) and PNM (right panels) in SB (red lines), MS96 (blue lines) and MS90 (cyan lines) at densities of $\rho = 0.07$ and -30.14 fm^{-3}.

Therefore, for the HugenholtzVan Hove (HVH) theorem we have:

$$\frac{p}{\rho} + \varepsilon = \sum_{i=n,p} (x_i \epsilon_{ph}(P_{Fi})) \tag{11}$$

where $\varepsilon = \frac{e}{\rho}$, $x_i = \frac{\rho_i}{\rho} i$, and $\epsilon_{ph}(P_{Fi}) = \frac{P_{Fi}^2}{2B} + U$ are the energy per particle, the relative fraction, and the Fermi energy in $P_{Fi} = (\frac{3h^3}{8\pi}\rho_i)^{1/3}$ for the ith nucleon, respectively. Another significant quantity that has an inevitable effect on determining the EOS of nuclear matter is the symmetry energy E_{sym} (the symmetry free energy F_{sym}), whose exact and approximate values can be calculated (Ghazanfari Mojarrad and Mousavi Khoroshtomi, 2017) in Eqs. (12) to (15), respectively:

$$E_{sym}(\rho, T) = \frac{1}{2} \frac{\partial^2 \left(\frac{e}{\rho}\right)}{\partial \delta^2}\Big|_{\delta=0} \tag{12}$$

$$E_{sym}(\rho, T) \simeq \frac{e(\delta = 1) - e(\delta = 0)}{\rho} \tag{13}$$

and

$$F_{sym}(\rho, T) = \frac{1}{2} \frac{\partial^2 \left(\frac{f}{\rho}\right)}{\partial \delta^2}\Big|_{\delta=0} = \lim_{\delta \to 0} \frac{\mu_n(\rho, T, \delta) - \mu_p(\rho, T, \delta)}{4\delta} \tag{14}$$

$$F_{sym}(\rho, T) \simeq \frac{f(\delta = 1) - f(\delta = 0)}{\rho} \tag{15}$$

Adopting the dimensionless parameter $x = \frac{\rho - \rho_0}{3\rho_0}$, one can determine the parameters of slope $L_{sym}^{(E)}$ and curvature $K_{sym}^{(E)}$, which show the dependence of the symmetry energy on the density:

$$E_{sym}(\rho, T) = E_{sym}(\rho_0, T) + L_{sym}^{(E)} x + \frac{K_{sym}^{(E)}}{2} x^2 + \bigcirc(x^3) \tag{16}$$

$$\longrightarrow L_{sym}^{(E)}(T) = 3\rho_0 \frac{\partial E_{sym}(\rho, T)}{\partial \rho}\Big|_{\rho=\rho_0}$$

$$K_{sym}^{(E)}(T) = 9\rho_0 \frac{\partial E_{sym}(\rho, T)}{\partial \rho^2}\Big|_{\rho=\rho_0} \tag{17}$$

In addition, the parameters of slope $L_{sym}^{(F)}$ and curvature $K_{sym}^{(F)}$ can be determined based on the symmetry free energy expansion:

$$F_{sym}(\rho, T) = F_{sym}(\rho_0, T) + L_{sym}^{(F)} x + \frac{K_{sym}^{(F)}}{2} x^2 + \bigcirc(x^3) \tag{18}$$

$$\longrightarrow L_{sym}^{(F)}(T) = 3\rho_0 \frac{\partial F_{sym}(\rho, T)}{\partial \rho}\Big|_{\rho=\rho_0}$$

$$K_{sym}^{(F)}(T) = 9\rho_0 \frac{\partial F_{sym}(\rho, T)}{\partial \rho^2}\Big|_{\rho=\rho_0} \tag{19}$$

On the other hand, for the thermodynamic stability of nuclear matter, one can introduce the curvature matrix f_{ij} as

$$\begin{pmatrix} \frac{\partial^2 f}{\partial \rho_n^2} & \frac{\partial^2 f}{\partial \rho_n \partial \rho_p} \\ \frac{\partial^2 f}{\partial \rho_p \partial \rho_n} & \frac{\partial^2 f}{\partial \rho_p^2} \end{pmatrix} \begin{pmatrix} \delta\rho_n^{\pm} \\ \delta\rho_p^{\pm} \end{pmatrix} = \lambda^{\pm} \begin{pmatrix} \delta\rho_n^{\pm} \\ \delta\rho_p^{\pm} \end{pmatrix} \tag{20}$$

imposing that both the determinant and trace of the curvature matrix f_{ij} are positive:

$$Tr(f_{ij}) = \lambda_+ + \lambda_- \geq 0 \tag{21}$$

$$Det(f_{ij}) = \lambda_+\lambda_- \geq 0 \tag{22}$$

where

$$\lambda_\pm = \frac{1}{2}\Big(Tr(f_{ij}) \pm \big(Tr(f_{ij})^2 - 4Det(f_{ij})\big)^{1/2}\Big) \tag{23}$$

$$\frac{\partial\rho_i^\pm}{\partial\rho_j^\pm} = \frac{\lambda_\pm - f_{jj}}{f_{jj}}, \qquad (i,j = n,p) \tag{24}$$

Therefore, when the conditions of Eqs. (21) and (22) are established, it can be concluded from Eq. (23) that $\lambda_\pm$ becomes positive. The positive curvature of f in the pure chemical direction $\delta\rho_n - \delta\rho_p = \frac{1}{2}\rho\delta\delta$ suggests that λ_+ remains positive (Ghaemmaghami and Mojarrad, 2022):

$$\lambda_- < \frac{\partial^2 f}{\partial\rho_n^2} = \frac{4}{\rho^2}\frac{\partial^2 f}{\partial\delta^2} = \frac{8}{\rho}F_{sym} < \lambda_+ \Longrightarrow \lambda_+ > 0 \tag{25}$$

In addition, the convexity of f in the pure mechanical direction $\delta\rho_n = \frac{\rho_n}{\rho_p}\delta\rho_p = \frac{1}{2}(1+\delta)(\delta\rho)$ leads to $(\frac{\partial P}{\partial p})_{T,\delta} > 0$ (Ghaemmaghami and Mojarrad, 2022). According to the all theoretical predictions, adopting $|\lambda_-| < \lambda_+$ in Eq. (23) ensures that $Tr(f_{ij})$ remains positive, even in cases of system instability (Margueron and Chomaz, 2003; Vidana and Polls, 2008). Within the instability region, one can conclude that the negativity of $Det(f_{ij})$ indicates that $(\frac{\partial P}{\partial p})_{T,\delta}$ and $(\frac{\partial \mu_p}{\partial \delta})_{T,p}$ cannot both concurrently represent independent types of instability, since

$$Det(f_{ij}) = \frac{2}{\rho_n\rho}\Big[(\frac{\partial P}{\partial p})_{T,\delta}(\frac{\partial \mu_p}{\partial \delta})_{T,p}\Big] \leq 0 \tag{26}$$

3 Results and Discussion of numerical methods

In order to present the statistical aspect of this model, Fig. 1 shows the effective energy of single particle $\epsilon_{ph} = \frac{p^2}{2B} + U$ as a function of wavenumber $K = \frac{p}{\hbar}$ for SNM and PNM at temperatures $T = 0$ MeV and $T = 10$ MeV . In general, ϵ_{ph} is significantly affected by the density and change of the system from SNM to PNM, while its temperature dependence is negligible. As shown, ϵ_{ph} has a stronger dependence on density at low wavenumbers. Based on the results, the single particle effective energy of neutrons in the Fermi momentum and at zero temperature is equal to the corresponding chemical potential , which confirms the HVH theorem in Eq. (11). As demonstrated, each curve obtained by the SB interaction, in comparison to the MS96 and MS90 interactions, exhibits a similar trend, while displaying a stronger dependence on the wavenumber. Meanwhile, the inner panel displays the behavior of the ratio of effective mass B (in units of the average nucleonic mass $\bar{m}$) versus the density, showing a decrease in this ratio as density increases. In addition, unlike the results reported in Ref. (Ghazanfari Mojarrad and Mousavi Khoroshtomi, 2017), the ratio $\frac{B}{\bar{m}}$ is independent of the asymmetric parameter and temperature.

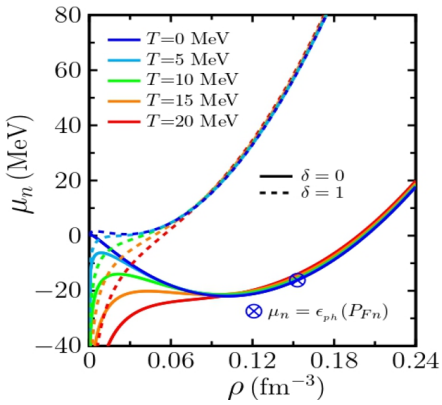

Figure 2: Neutron chemical potential as a function of density at temperatures $T = 0, 5, 10, 15$, and 20 MeV for SNM (solid lines) and PNM (dashed lines).

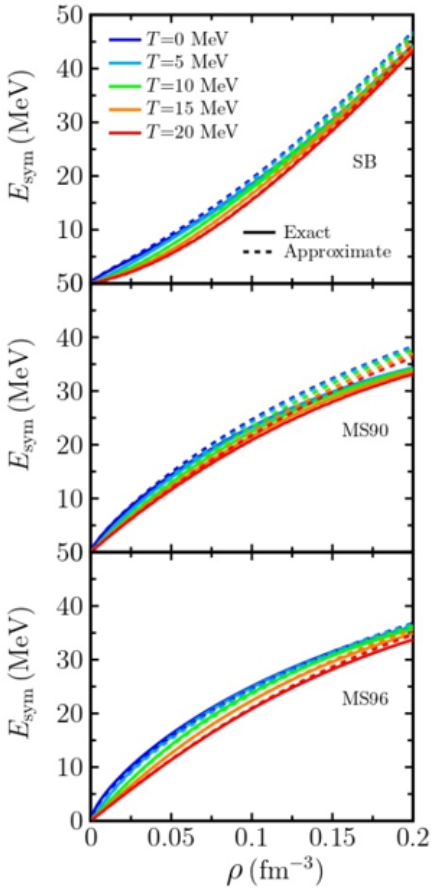

Figure 3: Symmetry energy as a function of density at temperatures $T = 0, 5, 10, 15$, and 20 MeV for the SB interaction (top panel), MS90 interaction (middle panel), and MS96 interaction (bottom panel) for exact (solid lines) and approximate (dashed lines) cal-culations.

Studying the chemical potential is crucial in order to understand the thermodynamics of nuclear matter. Therefore, in Fig. 2, we show the neutron chemical potential μ_n as a function of density for SNM and PNM at different temperatures. Generally, μ_n increases with increasing density for PNM, while for SNM a decreasing trend can be observed at lower densities and temperatures. Our result indicates that the HVH theorem is validated at

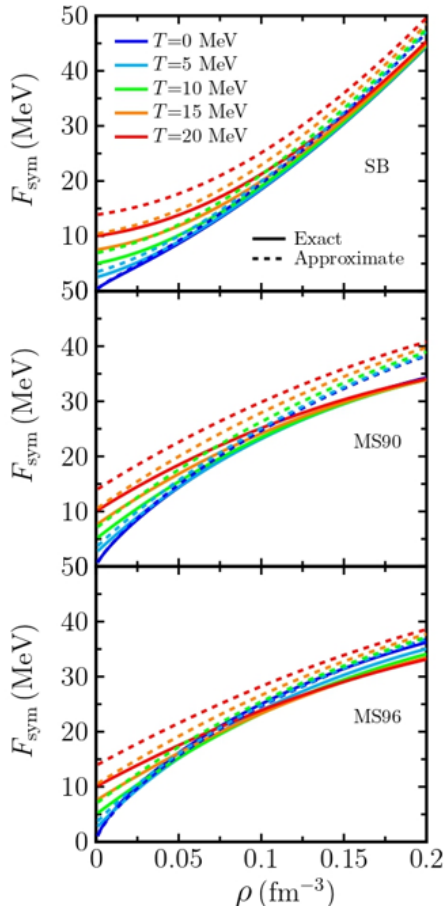

Figure 4: Symmetry free energy as a function of density at temperatures $T = 0, 5, 10, 15$, and 20 MeV for the SB interaction (top panel), MS90 interaction (middle panel), and the MS96 interaction (bottom panel) for exact (solid lines) and approximate (dashed lines) calculations.

the saturation point of the SNM, characterized by the conditions $\rho = \rho_0$, $\varepsilon = \varepsilon_0$, and $P = 0$. Furthermore, compared to Ref. (Ghaemmaghami and Mojarrad, 2022), μ_n changes more rapidly as a function of the density.

The quantities of symmetry energy and symmetry free energy play a key role in understanding the basic properties of the nuclear force. Hence, in Figs. 3 and 4, the symmetry energy E_{sym} and the symmetry free energy F_{sym} are calculated as a function of density not only for the BS interaction but also for its extensions, i.e. the MS90 and MS96 interactions proposed in Ref. (Ghaemmaghami and Mojarrad, 2022). As the density increases, the SB interaction demonstrates a stiffer behavior in the symmetry and symmetry-free energy, compared to MS90 and MS96 at different temperatures. In addition, symmetry energy (symmetry free energy) decreases (increases) with increasing temperature. In general, with increasing temperature, the differences between the exact and approximate results become more significant.

The parameters of slope $L^{(E)}_{sym}(L^{(F)}_{sym})$ and curvature $K^{(E)}_{sym}(K^{(F)}_{sym})$ specify the dependence of symmetry energy (symmetry free energy) on density. In other words, these quantities play a crucial role in determining the stiffness of the symmetry energy. Therefore, in Figs. 5 and 6, the parameters of slope and curvature are shown as a function of temperature. Our findings indicate that these parameters in SB are appreciably larger than those in MS90 and MS96. As a general trend, $L^{(E)}_{sym}$ demonstrates an increase with rising temperature with $L^{(F)}_{sym}$ exhibiting a decrease. Overall, contrary to $K^{(E)}_{sym}$, $K^{(F)}_{sym}$ shows an increasing trend with temperature. Consequently, the dissimilarity between the behavior of the symmetry energy in the SB interaction and the one in the MS interactions can be ascribed to the positivity (negativity) of the curvature parameters in SB (MS).

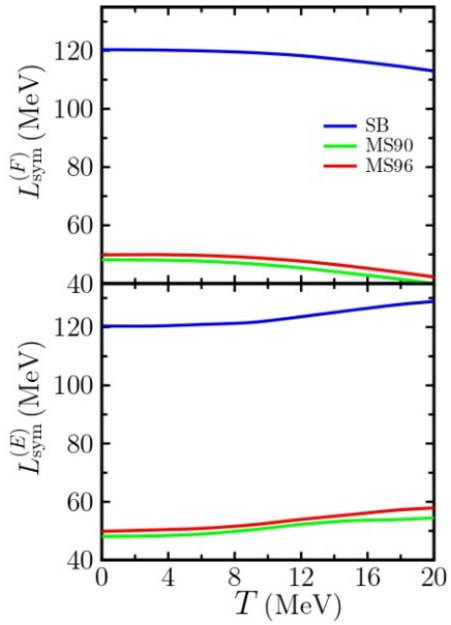

Figure 5: Slope parameter of symmetry free energy (top Panel) and symmetry energy (bottom panel) as a function of temperature.

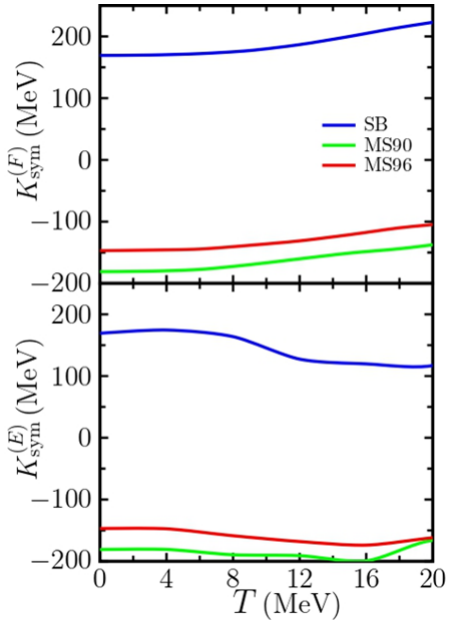

Figure 6: Curvature parameter of symmetry free energy (top panel) and symmetry energy (bottom panel) as a function of temperature.

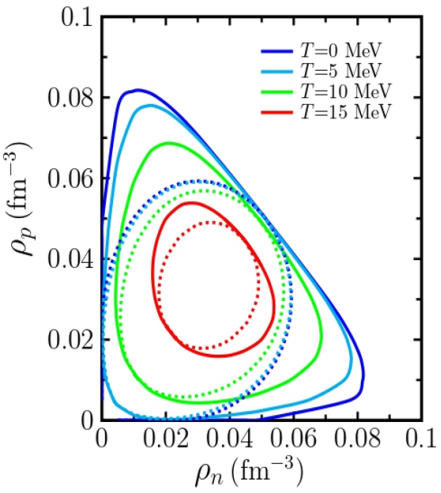

Figure 7: Total instability contours (solid lines) at temperatures $T = 0, 5, 10$, and 15 MeV in the $\rho_p - \rho_n$ plain. The regions associated with the instability in the pure mechanical direction are specified by the dotted contours.

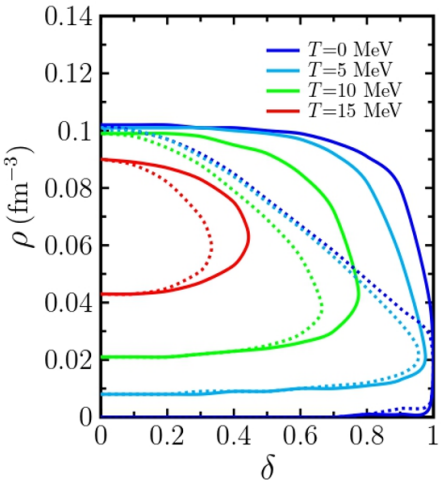

Figure 8: Total instability contours (solid lines) at temperatures $T = 0, 5, 10$, and 15 MeV in the $\rho - \delta$ plain. The regions associated with the instability in the pure mechanical direction are specified by the dotted contours.

Figuers 7 and 8 depict the region of total instability, where $Det(f_{ij}) < 0$, in the $p - \delta$ and $\rho_p - \rho_n$ planes. In addition, the region corresponding to the instability in the pure mechanical direction is also specified in these figures. The findings demonstrate that the instability region shrinks significantly with increasing temperature, disappearing completely at the critical temperature of $T_c = 17.2$ MeV. In all cases, the region of instability in the pure mechanical direction is inside the total instability region. As it has been shown, the region of instability in the pure mechanical direction has been significantly expanded in comparison with Ref. (Ghaemmaghami and Mojarrad, 2022).

Figure 9 depicts the ratio $\frac{\delta\rho_p^-}{\delta\rho_n^-}$, which represents the instability corresponding to the eigenvalue λ_-, as a function of δ at various temperatures. Our results show that the dominant nature of the instability is mechanical, since the ratio $\frac{\delta\rho_p^-}{\delta\rho_n^-}$ is always greater than the ratio $\frac{\rho_p}{\rho_n}$. With increasing temperature, the ratio $\frac{\delta\rho_p^-}{\delta\rho_n^-}$ decreases, leading to more noticeable thermal effects at lower densities. In general, the ratio of $\frac{\delta\rho_p^-}{\delta\rho_n^-}$ versus δ has a decreasing behavior at constant density. Additionally, the convergence of all isothermal curves for SNM at $\frac{\delta\rho_p^-}{\delta\rho_n^-} = 1$, indicates a one-component structure and pure mechanical instability driven by nucleon density fluctuations, highlighting the significant role of these fluctuations in the instability.

In order to compare the outcomes of the SB interaction in the instability, the ratio $\frac{\delta\rho_p^-}{\delta\rho_n^-}$ as a function of ρ is presented in Fig. 10. Our results regarding the SB interaction, being consistent with the NL3 model (Avancini et al., 2006), indicate that the ratio $\frac{\delta\rho_p^-}{\delta\rho_n^-}$ increases with ρ at a constant δ due to not incorporating any density-dependent term in the internucleon interactions. However, in the case of MS (MS90, MS96) (Ghaemmaghami and Mojarrad, 2022) interactions and the BHF model (Vidana and Polls, 2008), where the density-dependent effects between nucleonnucleon potentials are taken into account, the ratio $\frac{\delta\rho_p^-}{\delta\rho_n^-}$ shows an initial increase with increasing ρ at constant δ and then follows a decrease.

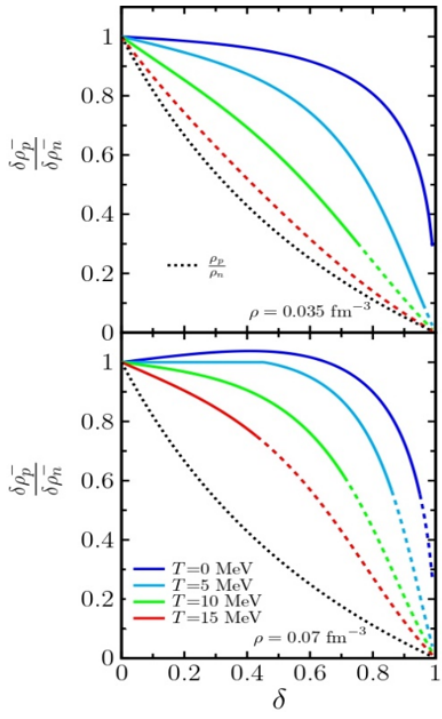

Figure 9: Ratio $\frac{\delta\rho_p^-}{\delta\rho_n^-}$ as a function of asymmetric parameter at temperatures $T = 0, 5, 10$, and 15 MeV for densities $\rho = 0.035$ MeV.fm^{-3} MeV.fm^{-3} (top panel) and $\rho = 0.07$ MeV.fm^{-3} (bottom panel). The short dashes are associated with $\lambda_- > 0$, and the long dashes show the ratio $\frac{\rho_p}{\rho_n}$.

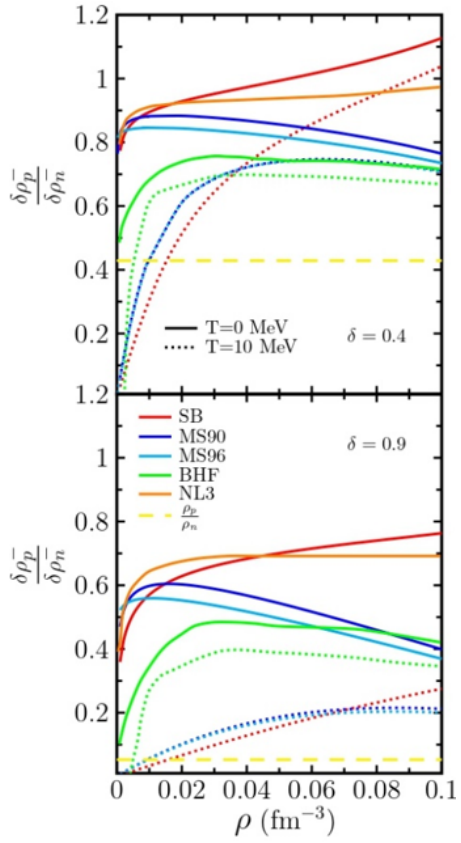

Figure 10: Ratio $\frac{\delta\rho_p^-}{\delta\rho_n^-}$ as functions of density for asymmetric parameters $\delta = 0.4$ (top panel) and $\delta = 0.4$ (bottom panel). The long dashes show the ratio $\frac{\rho_p}{\rho_n}$.

4 Summary and conclusion

In this research, we have investigated the thermodynamic properties of nuclear matter with special attention to the symmetry energy, symmetry free energy, and their role in thermodynamic instabilities of ANM in the framework of the Thomas-Fermi statistical model using the SB interaction. In the first stage, the effective single-particle energy has been determined for the different thermodynamic states, while the nucleon density has the strongest effect on this quantity. The behavior of the neutron chemical potential in SNM and PNM has also been probed, by which the compatibility of the HVH theorem in this model has been examines.The accurate and approximate calculations of the symmetry energy and symmetry free energy have evidently confirmed the stiffer behavior of these quantities in the SB interaction, compared to the MS interactions at different temperatures. In addition, examining the slope and curvature parameters of the symmetry energy and symmetry free energy has shown that density-dependent terms in the MS interactions lead to a significant difference from the results obtained in the SB interaction. Additionally, our investigations have demonstrated that temperature exerts a dominant influence in the elimination of unstable regions within the phase diagrams. On the other hand, the mechanical instability region becomes larger in the SB interaction than that given by the MS interactions due to the stiffer behavior of the symmetry free energy. Moreover, the SB interaction behaves similarly to the NL3 model in the direction toward instability, while the density-dependent effects in MS interactions and the BHF model lead to a different behavior. Finally, this study can provide an undinaible basis for a profound research on the liquid-gas phase transition in the future.

Acknowledgements

Authors would like to thank University of Kashan for supporting this project under the grant num-ber 1312170/1 provided by the Research Council.

Conflict of Interest

The authors declare no potential conflict of interest regarding the publication of this work.

References

Avancini, S., Brito, L., Chomaz, P., et al. (2006). Spinodal instabilities and the distillation effect in relativistic hadronic models. *Physical Review CNuclear Physics*, 74(2):024317.

Baldo, M., Fiasconaro, A., Song, H., et al. (2001). High density symmetric nuclear matter in the Bethe-Brueckner-Goldstone approach. *Physical Review C*, 65(1):017303.

Bandyopadhyay, D. and Samaddar, S. (1988). Energy dependent potential in nuclear collisions. *Nuclear Physics A*, 484(2):315–336.

Bandyopadhyay, D., Samanta, C., Samaddar, S., et al. (1990). Thermostatic properties of finite and infinite nuclear systems. *Nuclear Physics A*, 511(1):1–28.

Brandow, B. H. (1967). Linked-cluster expansions for the nuclear many-body problem. *Reviews of Modern Physics*, 39(4):771.

Camenzind, M. (2007). *Compact objects in astrophysics*. Springer.

Drischler, C., Hebeler, K., and Schwenk, A. (2016). Asymmetric nuclear matter based on chiral two-and three-nucleon interactions. *Physical Review C*, 93(5):054314.

Fedoseew, A. and Lenske, H. (2015). Thermal properties of asymmetric nuclear matter. *Physical Review C*, 91(3):034307.

Ghaemmaghami, S. and Ghazanfari Mojarrad, M. (2023). Thermal effects on the baryon–quark phase transition in hot hybrid neutron stars: a statistical mean-field baryonic model with the standard NJL model for deconfined quarks. *The European Physical Journal Plus*, 138(11):1–12.

Ghaemmaghami, S., Khoshi, M., and Mojarrad, M. G. (2023). Influence of a phase-space extension of nuclear forces on the sharp baryon-quark phase transition in hybrid neutron stars. *The European Physical Journal Plus*, 138(5):1–14.

Ghaemmaghami, S. and Mojarrad, M. G. (2022). A statistical model for the thermodynamic instabilities of asymmetric nuclear matter. *The European Physical Journal A*, 58(12):255.

Ghazanfari Mojarrad, M. and Arabsaeidi, R. (2016). Hyperon-rich matter in a two-solar-mass neutron star within the Thomas-Fermi approximation. *International Journal of Modern Physics E*, 25(12):1650102.

Ghazanfari Mojarrad, M. and Mousavi Khoroshtomi, S. (2017). Thomas–Fermi approximation for the equation of state of nuclear matter: A semi-classical approach from the Landau Fermi-Liquid theory. *International Journal of Modern Physics E*, 26(06):1750038.

Ghazanfari Mojarrad, M. and Ranjbar, J. (2019). Hybrid neutron stars in the Thomas-Fermi theory. *Physical Review C*, 100(1):015804.

Hempel, M., Fischer, T., Schaffner-Bielich, J., et al. (2012). New equations of state in simulations of core-collapse supernovae. *The Astrophysical Journal*, 748(1):70.

Margueron, J. and Chomaz, P. (2003). A unique spinodal region in asymmetric nuclear matter. *Physical Review C*, 67(4):041602.

Mojarrad, M. G. and Ranjbar, J. (2020). Thomas–Fermi approximation in the phase transition of neutron star matter from β-stable nuclear matter to quark matter. *Annals of Physics*, 412:168048.

Mojarrad, M. G. and Razavi, N. (2019). Proto-neutron stars in the Thomas-Fermi theory. *Nuclear Physics A*, 986:133–149.

Mojarrad, M. G., Razavi, N., and Vaezzade, S. (2018). Thomas–Fermi approximation for β-stable nuclear matter in the Landau Fermi-liquid theory. *Nuclear Physics A*, 980:51–66.

Moshfegh, H. and Ghazanfari Mojarrad, M. (2013). Strange baryonic matter in the Thomas-Fermi theory. *The European Physical Journal A*, 49(1):1.

Moshfegh, H. and Mojarrad, M. G. (2011). Thermal properties of baryonic matter. *Journal of Physics G: Nuclear and Particle Physics*, 38(8):085102.

Myers, W. and Swiatecki, W. (1990). A Thomas-Fermi model of nuclei. Part I. Formulation and first results. *Annals of physics*, 204(2):401–431.

Pons, J., Reddy, S., Prakash, M., et al. (1999). Evolution of proto-neutron stars. *The Astrophysical Journal*, 513(2):780.

Prakash, M., Bombaci, I., Prakash, M., et al. (1997). Composition and structure of protoneutron stars. *Physics Reports*, 280(1):1–77.

Randrup, J. and de Lima Medeiros, E. (1991). Model for statistical properties of nuclear systems at finite temperature. *Nuclear Physics A*, 529(1):115–140.

Ranjbar, J. and Ghazanfari Mojarrad, M. (2021). Hybrid neutron stars with the Thomas-Fermi approximation and nonlocal Nambu–Jona-Lasinio model. *Physical Review C*, 104(4):045807.

Razavi, N. and Mojarrad, M. G. (2023). Hot dense nuclear matter with the Thomas-Fermi approximation. *Nuclear Physics A*, 1029:122556.

Seyler, R. and Blanchard, C. (1961). Classical Self-Consistent Nuclear Model. *Physical Review*, 124(1):227.

Strobel, K. and Weigel, M. K. (2001). On the minimum and maximum mass of neutron stars and the delayed collapse. *Astronomy & Astrophysics*, 367(2):582–587.

Vidana, I. and Polls, A. (2008). Spinodal instabilities of asymmetric nuclear matter within the Brueckner–Hartree–Fock approach. *Physics Letters B*, 666(3):232–238.

Xu, J., Chen, L.-W., Li, B.-A., et al. (2007). Temperature effects on the nuclear symmetry energy and symmetry free energy with an isospin and momentum dependent interaction. *Physical Review CNuclear Physics*, 75(1):014607.

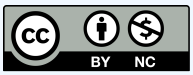

To cite this article:

Ghaemmaghami, S. Alireza and Ghazanfari Mojarrad, M. (2025). Nuclear symmetry energy and its role in the thermodynamic instabilities of nuclear matter using an ab initio statistical approach. *Radiation Physics and Engineering*, 6(3), 9-16. doi: 10.22034/rpe.2024.455720.1195

DOI: 10.22034/rpe.2024.455720.1195

To link to this article: https://doi.org/10.22034/rpe.2024.455720.1195